Arsenic behavior across soil-water interfaces in paddy soils: coupling, decoupling and speciation

YUAN, Zhao-Feng, GUSTAVE, Williamson, BOYLE, John, SEKAR, Raju <http://orcid.org/0000-0002-1182-9004>, BRIDGE, Jonathan <http://orcid.org/0000-0003-3717-519X>, REN, Yuxiang, TANG, Xianjin, GUO, Bin and CHEN, Zheng

Title: Arsenic behavior across soil-water interfaces in paddy soils: coupling, decoupling and speciation

Names of authors: Zhao-Feng Yuan [1, 2], Williamson Gustave [1, 2, 3], John Boyle [4], Raju Sekar [5], Jonathan Bridge [6], Yuxiang Ren [1], Xianjin Tang [7], Bin Guo [8 *] and Zheng Chen [1 *]

[1] Department of Health and Environmental Sciences, Xi'an Jiaotong-Liverpool University, 111 Ren'ai Road, Suzhou, Jiangsu 215123, China.

[2] Department of Environmental Science, University of Liverpool, Brownlow Hill, Liverpool L69 7ZX, UK.

[3] Chemistry, Environmental & Life Sciences, University of The Bahamas, New Providence, Nassau, The Bahamas.

[4] Department of Geography & Planning, University of Liverpool, Roxby Building, Liverpool, L69 7ZT, UK.

[5] Department of Biological Sciences, Xi'an Jiaotong-Liverpool University, 111 Ren'ai Road, Suzhou, Jiangsu 215123, China.

[6] Department of Natural and Built Environment, Sheffield Hallam University, Howard St, Sheffield S1 1WB, UK.

[7] Institute of Soil and Water Resources and Environmental Science, Zhejiang Provincial Key Laboratory of Agricultural Resources and Environment, Zhejiang University, 866 Yuhangtang Road, Hangzhou 310058, China.

[8] Institute of Environment, Resource, Soil and Fertilizer, Zhejiang Academy of Agricultural Sciences, Hangzhou, 310021, China.

[*] **Corresponding author**: Bin Guo (Email: ndgb@163.com); Zheng Chen (E-mail: ebiogeochem@outlook.com or Zheng.Chen@xjtlu.edu.cn; Tel: +86-512-81880471; fax: +86-512-88161899).

Abstract

The sharp redox gradient at soil-water interfaces (SWI) plays a key role in controlling arsenic (As) translocation and transformation in paddy soils. When Eh drops, As is released to porewater from solid iron (Fe) and manganese (Mn) minerals and reduced to arsenite. However, the coupling or decoupling processes operating within the redox gradient at the SWI in flooded paddy soils remain poorly constrained due to the lack of direct evidence. In this paper, we reported the mm-scale mapping of Fe, As and other associated elements across the redox gradient in the SWI of five different paddy soils. The results showed a strong positive linear relationship between dissolved Fe, Mn, As, and phosphorus (P) in 4 out of the 5 paddy soils, indicating the general coupling of these elements. However, decoupling of Fe, Mn and As was observed in one of the paddy soils. In this soil, distinct releasing profiles of Mn, As and Fe were observed, and the releasing order followed the redox ladder. Further investigation of As species showed the ratio of arsenite to total As dropped from 100% to 75.5% and then kept stable along depth of the soil profile, which indicates a dynamic equilibrium between arsenite oxidization and arsenate reduction. This study provides direct evidence of multi-elements' interaction along redox gradient of SWI in paddy soils.

Keywords: arsenic, iron, profile, paddy soil, coupling, decoupling

1. Introduction

Paddy fields globally represent artificial wetlands, supporting the growth of rice (Bouman and Tuong, 2001). Paddy agriculture for the production of rice involves intermittent flooding to favor the growth of rice and in some cases to reduce the bioavailability of cadmium (Hu et al., 2015). During the flooding stage, redox-sensitive elements in the soil, such as iron (Fe) and manganese (Mn), may become mobile from the solid into the liquid phase (Xu et al., 2017; Zhang et al., 2018), and lead to dissolution of the sorbates (e.g. arsenic (As), and phosphorus (P)) bound on the solid phase (act as sorbents) (Darland and Inskeep, 1997; Polizzotto et al., 2008). Other redox-sensitive elements, such as sulfur (S), may become immobile from the liquid to solid phase, and result in immobilization of dissolved elements through co-precipitation (e.g. FeS, As_2S_3) or adsorption (Burton et al., 2008). Among the noted elements, the mobilization of As is of particular concern since rice plants can efficiently uptake and accumulate As in their rice grains (Honma et al., 2016; Gustave et al., 2019a). This poses a threat to human health since long-term As exposure is known to cause cancer and organ failure (Meharg, 2004; Roberts et al., 2010). Understanding the biogeochemical cycling of As in paddy soils under heterogeneous and transient geochemical conditions during flooding and drainage is therefore of high importance in predicting and thus mitigating its uptake into food crops.

Arsenic behavior in saturated soils is closely coupled to that of Fe oxides. This occurs because Fe oxides provide the main adsorption sites for As (Zobrist et al., 2000; Chen et al., 2006; Tufano et al., 2008). When paddy soils are flooded, Fe oxides are reduced and dissolved by dissimilatory Fe reducing bacteria, leading to the simultaneous release of adsorbed As into porewater (Takahashi et al., 2004). The term "coupling of Fe and As" was used to describe this phenomenon, in which the release of Fe and As into the soil porewater shows a close positive correlation (Weber et al., 2010). In contrast, the term "decoupling of Fe and As" was defined to refer to the lack of a linear correlation between dissolved Fe and As concentrations (Weber et al., 2010).

Coupling of Fe and As has been well documented in soils, yet the decoupling process remains not well resolved (Weber et al., 2010; Bennett et al., 2012). To clarify the mechanisms regulating the potential decoupling of As and Fe, simplified water-Fe minerals-bacteria systems were employed (Tufano et al., 2008; Tufano and Scott, 2008; Weber et al., 2010), which indicated that coupling-decoupling is thermodynamically controlled. For example, Zobrist et al. identified *sulfurospirillum barnesii* was able to reduce adsorbed arsenate [As(V)] to arsenite [As(III)] without requiring dissolution of the host Fe oxides (Zobrist et al., 2000), which could be caused by an energy trade-off between reduction of adsorbed As(V) and host Fe minerals by microorganisms (Campbell et al., 2006) (Islam et al., 2004). However, to date this has not been confirmed in soils.

In saturated soils, it has been a challenge to distinguish the potential decoupling between Fe and As. Homogeneous saturated soils were frequently used to investigate the time-dependent behaviors of Fe and As (Masscheleyn et al., 1991; White et al., 2007; Weber et al., 2010; Das et al., 2016; Honma et al., 2016; Xu et al., 2017), yet the potential decoupling of As and Fe was only demonstrated in few deep aquifers (White et al., 2007; Das et al., 2016). In most cases, the time-series investigation is unable to capture the time points and/or hotspots that decoupling of Fe and As occurs. The unsuccessful identification of the decoupling process is not surprising, because the Fe reduction and As releasing usually happen in sequence with little temporal offset (Zhang et al., 2018). The dynamic change of Fe and As makes it hard to catch the appropriate time point, even if the decoupling of Fe and As occurs.

When flooded, the bulk soil becomes reduced owing to the abundant organic matters (Frenzel et al., 1992). At the same time, a stable redox gradient is formed between the O_2-rich surface water and subsurface soil, which could significantly influence the spatial distribution of redox-sensitive elements (Mucci et al., 2000; Widerlund and Davison, 2007; Arsic et al., 2018). Hence, the narrow but stable soil water interface (SWI) is an ideal place to study the coupling/decoupling processes of Fe and As along depth (Bennett et al., 2012; Gorny et al., 2015). Although As(V) reduction theoretically happened at higher redox potential (Eh) compared to Fe(III) (Borch et al., 2010), few studies have detected the spatial separation of Fe(II) and As species in SWI of natural soils. This could be attributed to the lack of a suitable

method to simultaneously measure fine-scale Fe, As and other associated elements across SWI (Gorny et al., 2015).

We recently developed a high-throughput method to simultaneously measure concentrations of multi-element (e.g. Fe, Mn, As, P and S) and their species across SWI (Yuan et al., 2019; Yuan et al., 2021). The SWI profiler used in our method shows a big advantage in non-destructively and repeatedly sampling of porewater at high-resolution (HR) (mm level) across SWI (Yuan et al., 2019), compared with traditional HR samplers (e.g. DET, peeper). The analytical technique in our method makes it possible to extract all interested parameters from volume-limited (~ 100 μL) samples collected by HR samplers (Yuan et al., 2021). In this study, the method was applied to reveal the coupling/decoupling process of Fe and As, as well as other associated elements, including Mn, S and P. Their profiles across the SWI in five paddy soils were mapped to 1) illustrate multi-element and Eh profiles in typical saturated paddy soils; 2) study the coupling/decoupling behaviors among the redox-sensitive elements and 3) reveal the As speciation process across the SWI.

2. Materials and methods

2.1 Reagents, materials and solutions. Analytical grade reagents were purchased from Aladdin Chemical Reagent Co., Ltd. (Shanghai, China), unless otherwise stated. Calibration standards, including As species, Fe, Mn, P, and S, were supplied by

Guobiao (Beijing) Testing & Certification Co., Ltd (Beijing, China). All solutions were prepared with ultrapure water (18.2 MΩ cm, Millipore Corp., Bedford, USA) deoxygenated by bubbling pure N_2 overnight.

Paddy soils with different levels of As (25.6 - 146 mg·kg^{-1}, Table S1) were collected from Wenshan (WS, 23°45'N, 105°26'E), Bijie (BI, 26°39'N, 105°47'E), Wuxue (WX, 29°59'N, 115°38'E), Shaoguan (SG, 25°6'N, 113°38'E) and Ganzhou (GZ, 25°30'N, 114°36'E), China. The plow layer soil (0 - 20 cm) was sampled and directly transported to the laboratory. Soils were wet mixed and sieved through a 1.0 mm diameter sieve. The wet sieved soils were mixed evenly and each soil type was added to three black plastic pots (inner diameter × height = 13 cm × 21 cm), with a soil depth of ~15 cm (total 15 pots). Table S1 shows the selected soil properties. The soils were flooded with ultrapure water and allowed to stabilize for 30 d in dark conditions, with a constant room temperature (22 °C) controlled by an air-conditioner.

2.2 Deployment and sampling of SWI profiler. The SWI profiler is a recently developed HR porewater sampler (Yuan et al., 2019). It has a sampling depth of 60 mm, with a spatial resolution of 1.7 mm. The SWI profiler was provided by Tidu Environment Inc. (Suzhou, China). Fifteen SWI profilers were inserted, one per pot, into the 15 pots comprising three replicates for each of WS, BI, WX, SG, and GZ paddy soils, such that the uppermost 10 mm of the profile length was in overlying water and the lower 50 mm buried in saturated soil. After 30 d of incubation,

porewater was sampled by SWI profiler. Eh profiles were simultaneously measured using a custom-made platinum micro-electrode with an Ag/AgCl reference electrode.

Before sampling, O_2-free ultrapure water was pumped into SWI profiler as the carrier solution, with an injection pump (TYD01, Lei Fu, China). After loading of the carrier solution, small ions and molecules can passively diffuse from porewater into SWI profiler driving by the concentration gradient. When the diffusion process reached equilibrium (after 24 h), the sample was pumped out by the injection pump (Fig. S1). The sample acidified with O_2-free HCl in the first sampling event was used for total elements analysis (Gustave et al., 2019b). In the second sampling event (24 h after the first one), the sample was preserved with O_2-free EDTA to complex metals (e.g. Fe), which would facilitate As species analysis under alkali conditions (Gallagher et al., 2001; Yuan et al., 2021). The collected samples were preserved at 4 °C fridge before downstream instrumental analysis.

2.3 Total elements analysis. Total Fe, Mn, As, P, and S obtained from SWI profiler samples were measured by inductively coupled plasma-mass spectrometry (ICP-MS, NexION 350X, PerkinElmer, Inc., Shelton, CT USA). The sample in 0.6 mL centrifuge tube (~ 100 µL) was introduced into ICP-MS by a PFA-200 Microflow Nebulizer for elemental analysis. The counts of $^{57}Fe^+$, $^{55}Mn^+$, $^{47}PO^+$, $^{48}SO^+$ and $^{91}AsO^+$ were recorded in dynamic reaction cell (DRC) or extended dynamic range (EDR) mode (Yuan et al., 2021). Spiked standards were measured after every 30 samples as a quality control measure.

The ICP-MS was optimized to the following conditions: DRC (O_2, gas flow: 1.0 $mL \cdot min^{-1}$); data only analysis; RF power: 1600W; plasma gas flow rate: 15 $L \cdot min^{-1}$; auxiliary gas flow: 1.2 $L \cdot min^{-1}$; nebulized gas flow: 0.90 $L \cdot min^{-1}$; nickel sampling and skimmer cones were used. A voltage parameter in EDR mode, called "rejection parameter a" (Rpa), was optimized to 0.01 for Fe, Mn and S to enable simultaneous measurement of majors (e.g. Fe, Mn, S) and traces (e.g. As) by ICP-MS, following the procedure described in Yuan et al. (2021).

2.4 Speciation of As in soil porewater. For As speciation analysis, the ~ 100 μL sample was manually loaded into a 25 μL sample loop of ion chromatography (IC, Dionex ICS-1100, Thermo Scientific, USA) (Yuan et al., 2021). The IC system consisted of an anion-exchange column (IonPac AS23, 250mm×4mm, Dionex). Twenty mM NH_4HCO_3 (pH = 10) were used as the mobile phase (Suzuki et al., 2009; Yuan et al., 2021). We expanded the comparison of As speciation in this study to digitized As species published in previous reports with the Engauge Digitizing software (version 11.3) used in a previous paddy soil study (Yuan et al., 2016).

2.5 Statistical analysis. Data were analyzed and plotted using R software (version 3.5.0). Standard errors were used to show the variance, and linear regression analysis was used to identify the coupling and decoupling process of different elements.

3. Results and discussion

189 **3.1 Vertical changes of Eh and elements across the SWI.** The Eh (*vs.* Ag/AgCl

190 reference electrode) and multi-element were measured and depicted in Fig. 1.

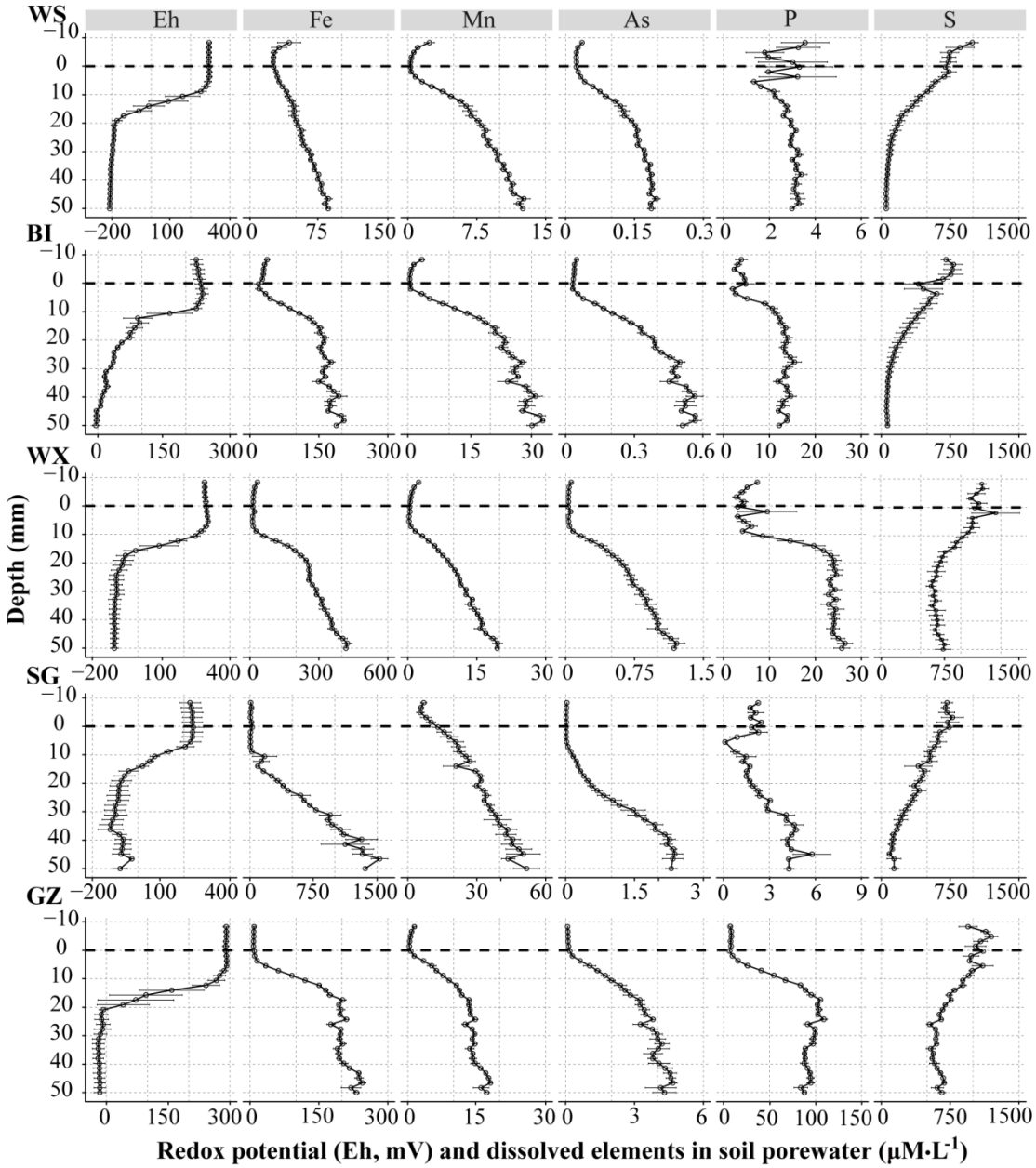

191

192 **Figure 1** Redox potential (Eh, mV, *vs.* Ag/AgCl reference electrode) and aqueous iron
193 (Fe), manganese (Mn), arsenic (As), phosphorus (P), sulfur (S) ($\mu M \cdot L^{-1}$) across the
194 soil-water interface. WS, BI, WX, SG and GZ represent soils collected from Wenshan,
195 Bijie, Wuxue, Shaoguan and Ganzhou paddies respectively. The black dotted line at
196 depth = 0 represents the soil-water interface. The error bar is standard error (n = 3).
197 Note the different axis scales used.

198 The Eh changed rapidly from highly oxidizing (~ 300 mV) to reducing conditions
199 along the depth of the SWI. However, the reducing levels varied among the different
200 paddy soils. Highly reducing condition (~ -150 mV) was observed in WS/WX/SG, yet
201 a relatively moderate one (~ -10 mV) in BI/GZ. This difference in Eh might be caused
202 by different physico-chemical properties of soils. Manganese and Fe are important
203 factors for regulating soil redox (Brannon et al., 1984; Xu et al., 2017). Here, we
204 found high Mn (6.32 $g \cdot Kg^{-1}$, WS) or Fe (> 70 $g \cdot Kg^{-1}$, WX/SG) alone was unable to
205 buffer the decrease of soil redox (Table S1). Buffering of soil redox was only
206 achieved with both high Fe and Mn (> 70 and 1.10 $g \cdot Kg^{-1}$) in BI/GZ. Although Mn is
207 believed to be the key for buffering soil redox (Xu et al., 2017), the formation of Fe
208 oxides coating with the nucleating agent is essential for nucleation and growth of Mn
209 oxides (Burns and Burns, 1975). Hence, Fe may also get involved in retarding soil
210 redox by affecting the reactivity of Mn.

211 Following Eh measurement, vertical profiles of Fe, Mn, As, P and S were
212 mapped by SWI profiler (Fig. 1). Dissolved Fe, Mn and As were almost undetectable
213 under oxidizing conditions, however their concentrations increased to 85.2 - 1359,
214 12.5 - 42.0 and 0.187 - 4.31 $\mu M \cdot L^{-1}$ respectively in reducing soils. In terms of the
215 release trend of those elements, they all showed a subsurface increase trend, which
216 agree well with previous reports of their typically vertical distributions along SWI (Di
217 et al., 2012; Wu et al., 2016a; Ma et al., 2017; Arsic et al., 2018). A similar trend was
218 also found on P. Similar to As (Xiu et al., 2016), P cycling is tightly tied to that of Fe

219 oxides in soils (Ding et al., 2016), due to Fe oxides provide the main adsorption sites
220 for P and As. The reductive mobilization of Fe, Mn, P and As was expected to
221 negatively correlate with Eh and S, nonetheless this was not always true for all the
222 paddy soils. For instance, the most As was mobilized in GZ which had a relatively
223 high Eh and S concentrations (~ -15.0 mV, ~ 635 $\mu M \cdot L^{-1}$ S, Fig. 1GZ), while the least
224 As was released in WS soil with an extremely low Eh and S (~ -200 mV, ~ 54.8
225 $\mu M \cdot L^{-1}$ S, Fig. 1WS). Similar observations to these results have been frequently
226 reported when using different soil samples (Bogdan and Schenk, 2008; Xu et al.,
227 2017). This is due to the complex process of As mobilization in soils. Although Fe
228 oxides are considered as a major agent controlling As mobilization (Xu et al., 2017), it
229 is also influenced by organic matter content, and formation of secondary minerals
230 along flooding (Bogdan and Schenk, 2008). Rich soil organic matter enhance As
231 release by accelerating biotic reduction of Fe oxides (Bogdan and Schenk, 2008). The
232 dissolved As could be re-immobilized by forming secondary minerals (like FeS, Fe_2S,
233 As_2S_3, siderite, vivianite etc.) (Bogdan and Schenk, 2008). Owing to the complex
234 biogeochemical processes involved in As mobilization, future studies should consider
235 multiple associated factors when assessing As mobilization.

236 Total dissolved S profiles have opposite trends as Fe, Mn, As and P, which
237 decreased rapidly from as high as 1000 $\mu M \cdot L^{-1}$ in oxidizing conditions to a
238 concentration of ~ 300 $\mu M \cdot L^{-1}$ in reducing soil conditions. High dissolved sulfide
239 might trigger the formation of thioarsenate/thioarsenite in soil porewater (Wang et al.,

2020b). However, due to thioarsenate/thioarsenite was strongly suppressed by high dissolved Fe in reducing soils (Wang et al., 2020b), thioarsenate/thioarsenite was not detected in the oxic-anoxic transition zone in this study.

The decrease of S is presumably caused by sulfate reduction (Pester et al., 2012), during which S(VI) is transformed to insoluble sulfide minerals by sulfate reducing bacteria (Wu et al., 2016a; Wu et al., 2016b). In soils investigated, up to 85% S was immobilized in WS/BI/SG, yet only 40% in WX/GZ. This difference of S fate might be caused by the activity of S-reducing/oxidizing bacteria (Pester et al., 2012). Higher activity of S(VI)-reducing bacteria tended to transform more soluble S(VI) to S(-II) minerals (like FeS, Fe_2S etc.) (Pester et al., 2012). By contrast, higher activity of S-oxidizing bacteria can sustain a larger S(VI) pool in saturated soils (Pester et al., 2012).

3.2 Coupling of As with Fe and Mn across SWI. Arsenic showed a significant linear relationship with Fe and Mn (Fig. 2 and Table S2). Excellent positive correlations were yielded in 4 out of the 5 soils (WS, BI, WX and GZ, $R^2 \geq 0.848$, $p < 0.01$), showing the tight coupling of As with Fe and Mn in typically natural soils and sediments (Anawar et al., 2004; Xu et al., 2017; Arsic et al., 2018). Among the 4 soils, a steeper slope of the relationship between As and Fe (~ 0.0202, respectively) was found in GZ soil than those in other soils (~ 0.00154) (Fig. 2A). The slopes may depend on the content of poorly crystalline Fe oxides, which have a high affinity for As (Tufano et al., 2008), and are subject to bioreduction by dissimilatory Fe reducing

bacteria (Zachara et al., 2002). Low content of poorly crystalline Fe oxides may retard As mobilization in the solid phase, even in soils rich in Fe (Khan et al., 2010).

Although close linear relationships of As and Mn were also found in WS, BI, WX and GZ soils except for SG soil (Fig. 2B), the role of Mn minerals may differ from Fe minerals. In the 4 soils, the Mn profiles are almost identical to Fe profiles, suggesting the reduction of Mn and Fe was controlled by the same group of microbial organisms (Myers and Nealson, 1988). However, the correlation of As and Fe/Mn in SG soil was not as well as those in other soils (Fig. 2). Furthermore, this result showed, unlike Fe reduction, Mn reduction doesn't follow with As release in the top layer of SG soil with low concentrations of both elements. We speculated the apparent decoupling of As with Mn may be caused by two reasons, 1) Fe oxides are still abundant when Mn minerals start to dissolute, which bind with the As desorbed from Mn minerals (Mitsunobu et al., 2020); 2) Mn minerals catalyze the oxidation of As(III) to As(V) (Chen et al., 2006), which is less mobile.

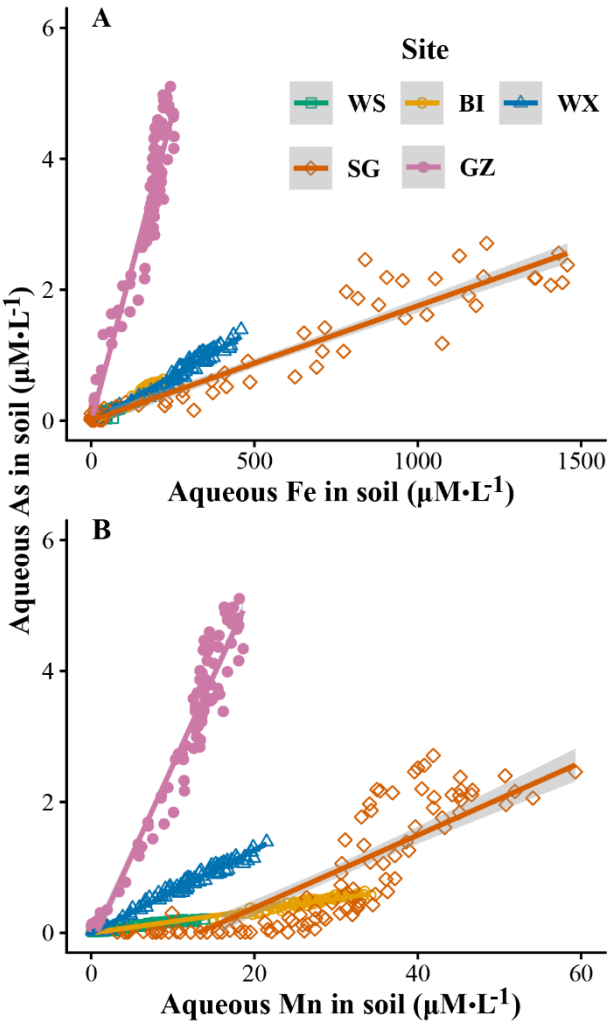

Figure 2 The correlation between vertical aqueous As with Fe (A) and Mn (B) (μM·L^{-1}) in paddy soils. Soils were collected from Wenshan (WS), Bijie (BI), Wuxue (WX), Shaoguan (SG) and Ganzhou (GZ) paddies.

In most cases, the cascade of Mn, As and Fe releasing to porewater along SWI is hard to spatially distinguish because their releasing zones are often overlapped (Dočekalová et al., 2002; Gao et al., 2006; Bennett et al., 2012; Arsic et al., 2018). Thus, the SG soil, which is high in Fe and Mn, is an excellent environmental sample to study the decoupling with the dominant coupling process. Regression residual analysis revealed the decoupling process happened in the oxic-anoxic transition zone

285 (Table S2). Much higher residuals were obtained in that zone of SG (residuals ≥ 0.265)
286 than in other soils with a similar regression slope (including WS, BI and WX,
287 residuals ≤ 0.0417).

288 **3.3 Speciation of As across SWI**. To reveal the arsenic speciation along Eh gradient
289 across SWI, we measured fine-scale As species profiles across the SWI of SG soil
290 (Fig. 3) and the As species at 3 depth in the other 4 soils (Table S3). Surprisingly, no
291 methyl arsenic was detected in all the samples, only As(III) and As(V) were found.
292 Although it is known that the methylation process of As is controlled by a family of
293 As(III) S-adenosylmethionine methyltransferases enzymes designated ArsM in
294 microbes or AS3MT in higher eukaryotes (Ajees and Rosen, 2015; Zhao et al., 2019),
295 the occurrence of methyl As is hard to predict in field samples. Chen et al. found that
296 the methyl As may only exist at a narrow Eh range because, when the Eh drops below
297 the Eh range, the methylotrophic methanogens capable of demethylating methyl As
298 outcompete those microbes possessing As methylating ability (Chen et al., 2019),
299 resulting in the disappearance of methyl As. According to this result, Eh only is not
300 sufficient to induce significant methyl As synthesis in the flooded soil system, as there
301 is no methylated As detected along the Eh gradient in all the soil samples. We
302 speculated that the availability of organic substrate and the functional microbial
303 community were the limiting factors in our case, more investigations are needed to
304 identify the micro-hotspot of methyl As in paddy soils.

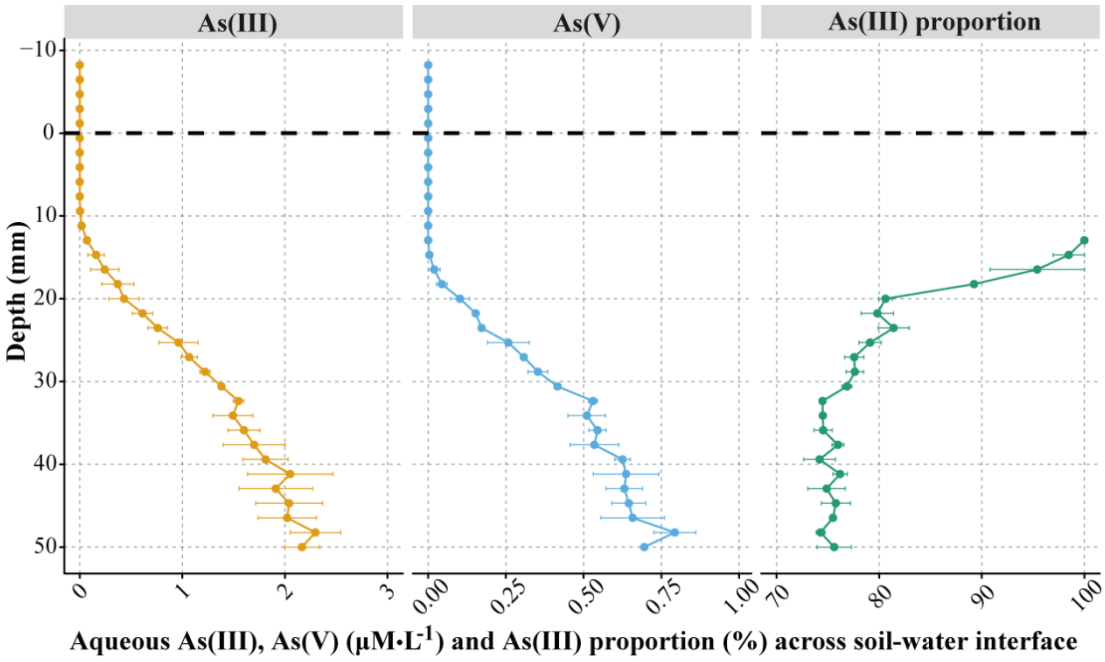

Figure 3 Profile of As species (μM·L^{-1}) and arsenite (As(III)) proportion across the soil-water interface in Shaoguan (SG) paddy. Two As species, including As(III) and arsenate (As(V)), were detected in soil porewater.

In SG soil, the concentrations of As(III) and As(V) remained almost undetectable in the oxic zone but increased rapidly from 0.0070 (9.4 mm below SWI) and 0.0091 (15 mm below SWI) μM·L^{-1} to as high as 2.2 and 0.75 μM·L^{-1} in reducing soils, respectively. A clear As(III) release spatially prior to As(V) is observed along SWI (Fig. 3). The similar phenomenon was only reported in marine sediments by using traditional soil slicing (Chaillou et al., 2003). Bennett et al. detected As(III) release was prior to that of ferrous Fe in the oxic-anoxic transition zone (Bennett et al., 2012). Those pieces of evidence suggested a decoupling of As(III) and Fe(II), and strong coupling of As(V) and Fe(II) in flooded soils and sediments.

Generally, three main processes were proposed to explain As releasing from solid Fe/Mn oxides to liquid phase. First, desorption of As from solid phase due to

repartitioning of adsorbed As between solid and liquid phase (Fig. 4A&E) (Zobrist et al., 2000; Williams et al., 2011). Second, the Fe(III) in the complex of Fe/Mn-As is reduced to Fe(II) following As release (Fig. 4B&F) (Xu et al., 2011; Gustave et al., 2018). Third, As(V) binding on Fe oxides is reduced to As(III), thus desorbed (Fig. 4C) (Zhang et al., 2018). According to the redox ladder (Borch et al., 2010), the third process is thermodynamically favored, which has been proven with pure minerals (Tufano et al., 2008; Tufano and Scott, 2008). To the best of our knowledge, the phenomenon has not been observed in saturated soils, because the latter two processes were considered to occur simultaneously (Weber et al., 2010). The data presented in Fig. 3 might be the first evidence from saturated soils supporting that the reduction of As(V) happens on solid minerals instead of in solution.

Based on the As(III) and As (V) profiles, the proportion of As(III) in total As was calculated and depicted in Fig. 3. The proportion change along SWI could be divided into three stages: 1) a rapid decrease from 100 to 80.6% in the first 10 - 20 mm topsoil; 2) a slow decrease from 80.6 to 75.5% in 20 - 30 mm soils and 3) a stable value (75.0 %) in deep soils (30 - 50 mm). In 30 - 50 mm below SWI (Fig. 3), the stable values of As concentration (As(III) and As(V): 2.40 and 0.498 $\mu M \cdot L^{-1}$ respectively) and As species in total As (75% As(III), 25% As(V)) indicate a dynamic equilibrium of aqueous As(III) oxidation *vs.* As(V) reduction and their immobilization *vs.* mobilization in deep soils. The immobilization process is most likely stimulated by the formation of secondary sulfide S(-II) minerals (e.g. FeS) (Fig. 4), since those

minerals can provide additional adsorption sites for dissolved As and other elements like P (Zhang and Selim, 2008; Wang et al., 2020a). The similar stable profile of As was frequently reported in anoxic freshwater sediments (Bennett et al., 2012; Di et al., 2012; Arsic et al., 2018). By contrast, a decrease of As along depth was captured in some marine sediments rich in S (Bennett et al., 2012). Under those conditions, the immobilization of As may outcompete the mobilization and lead to As decrease in anoxic soils when S(VI) reduction predominates.

It is interesting to note that, according to the Eh-pH diagram, all the inorganic As in Eh < 0 mV (*vs.* standard hydrogen electrode) should be As(III) under circumneutral conditions (Akter et al., **2005**). However, a considerable amount of As(V) (~ 25.0%) was observed in SG soil, and the proportion was independent of soil depth in the zone (Fig. 3). The persistent As(V) existence in reducing soils may represent a thermodynamic equilibration of four biogeochemical processes: 1) abiotic (by Mn oxides) or microbial oxidation of As(III) to As(V) (Fig. 4D) (Liu, 2006; Suda and Makino, 2016; Tong et al., 2019); 2) desorption of As(V) from the solid phase due to competition of adsorption sites by analogues (e.g. carbonate, bicarbonate, phosphate, dissolved organic matter) (Fig. 4E) (Zobrist et al., 2000; Grafe et al., 2001; Violante and Pigna, 2002; Anawar et al., 2004); 3) release of the adsorbed As(V) due to microbial reduction and solubilization of the host Fe oxides (Fig. 4F) (Tufano et al., 2008; Zhang et al., 2018); and 4) readily As(V) supply from humic acids (Fig. 4) (Anawar et al., 2003; Chaillou et al., 2003). To verify whether there is a

thermodynamic equilibration of As(III) and As(V) in soil porewater, we collected the As species data from publications using typically natural soils/sediments (Table S4). The results showed dissolved As under anoxic was usually dominated by As(III) , but significant As(V) (~ 20.0%) was observed in most cases (Chaillou et al., 2003; Zheng et al., 2003; Roberts et al., 2010; Somenahally et al., 2011; Hu et al., 2015; Shakoor et al., 2015; Kumar et al., 2016; Bondu et al., 2017; Xu et al., 2017; Arsic et al., 2018; Kazi et al., 2018; Lock et al., 2018; Wang et al., 2019).

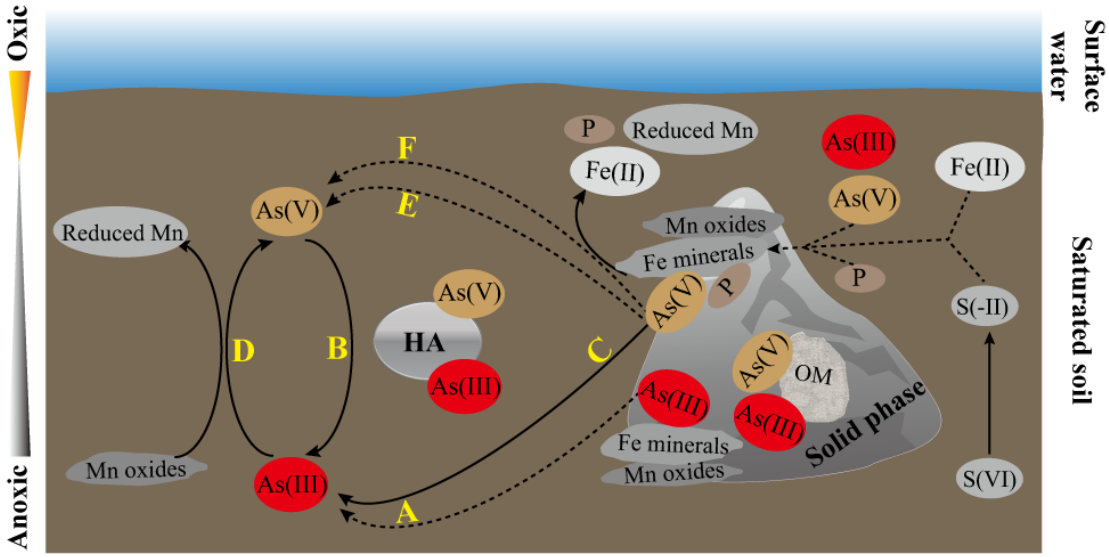

Figure 4 Diagram (nonspatial) depicting the processes controlling the behavior of multi-element in saturated soils. A-C) pathways contribute to As(III) enrichment in soil porewater; D-F) pathways contribute to As(V) enrichment in soil porewater. OM is solid organic matter, and HA is humic acids.

4. Conclusion

This study investigated vertical changes of Eh, Fe, Mn, As, P, S as well as As species across SWI in paddy soils. High-resolution (mm) mapping of total aqueous Fe, Mn,

As, P and S by SWI profiler visibly showed one-dimensional coupling and decoupling of As with Fe and Mn in different soils. Profiling of As species further identified As(III) excess was the main cause of the decoupling of As with Fe and Mn in the oxic-anoxic transition zone. Future studies, combining high-resolution mapping of multi-element with microbial community, are essential to improve the understanding of As behaviors in soils, sediments and other aquatic environments.

Conflict of Interest

The authors declare no conflict of interest.

Acknowledgements

This work was supported by the National Science Foundation of China (41571305, 41977320), Key Programme Special Fund of XJTLU (KSF-A-20). We want to thank the kind help of Fuyuan Liu for designing 3D printing model. We are grateful for the assistance of Yi-Li Cheng, Xiao Zhou, Xiao-Yan Zhang, and Liang-Ping Long with chemical analysis.

References

Ajees, A.A., Rosen, B.P., 2015. As(III) S-adenosylmethionine methyltransferases and other arsenic binding proteins. Geomicrobiol. J. 32, 570-576.

Akter, K.F., Owens, G., Davey, D.E., Naidu, R., 2005. Arsenic speciation and toxicity in biological systems. Reviews of environmental contamination and toxicology. Springer, pp. 97-149.

Anawar, H.M., Akai, J., Komaki, K., Terao, H., Yoshioka, T., Ishizuka, T., Safiullah, S., Kato, K., 2003. Geochemical occurrence of arsenic in groundwater of Bangladesh: sources and mobilization processes. J. Geochem. Explor. 77, 109-131.

Anawar, H.M., Akai, J., Sakugawa, H., 2004. Mobilization of arsenic from subsurface sediments by effect of bicarbonate ions in groundwater. Chemosphere 54, 753-762.

Arsic, M., Teasdale, P.R., Welsh, D.T., Johnston, S.G., Burton, E.D., Hockmann, K., Bennett, W.W., 2018. Diffusive gradients in thin films (DGT) reveals antimony and arsenic mobility differs in a contaminated wetland sediment during an oxic-anoxic transition. Environ. Sci. Technol. 52, 1118-1127.

Bennett, W.W., Teasdale, P.R., Panther, J.G., Welsh, D.T., Zhao, H., Jolley, D.F., 2012. Investigating arsenic speciation and mobilization in sediments with DGT and DET: a mesocosm evaluation of oxic-anoxic transitions. Environ. Sci. Technol. 46, 3981-3989.

Bogdan, K., Schenk, M.K., 2008. Arsenic in rice (*Oryza sativa* L.) related to dynamics of arsenic and silicic acid in paddy soils. Environ. Sci. Technol. 42, 7885-7890.

Bondu, R., Cloutier, V., Rosa, E., Benzaazoua, M., 2017. Mobility and speciation of geogenic arsenic in bedrock groundwater from the Canadian Shield in western Quebec, Canada. Sci. Total Environ. 574, 509-519.

415 Borch, T., Kretzschmar, R., Kappler, A., Cappellen, P.V., Gindervogel, M., Voegelin, A., Campbell, K.,
416 2010. Biogeochemical redox processes and their impact on contaminant dynamics. Environ. Sci.
417 Technol. 44, 15-23.
418 Bouman, B., Tuong, T.P., 2001. Field water management to save water and increase its productivity in
419 irrigated lowland rice. Agr. Water Manage. 49, 11-30.
420 Brannon, J., Gunnison, D., Smart, R., Chen, R., 1984. Effects of added organic matter on iron and
421 manganese redox systems in sediment. Geomicrobiol. J. 3, 319-341.
422 Burns, R.G., Burns, V.M., 1975. Mechanism for nucleation and growth of manganese nodules. Nature
423 255, 130-131.
424 Burton, E.D., Bush, R.T., Sullivan, L.A., Johnston, S.G., Hocking, R.K., 2008. Mobility of arsenic and
425 selected metals during re-flooding of iron- and organic-rich acid-sulfate soil. Chem. Geol. 253, 64-73.
426 Campbell, K.M., Malasarn, D., Saltikov, C.W., Newman, D.K., Hering, J.G., 2006. Simultaneous
427 microbial reduction of iron (III) and arsenic (V) in suspensions of hydrous ferric oxide. Environ. Sci.
428 Technol. 40, 5950-5955.
429 Chaillou, G., Schäfer, J., Anschutz, P., Lavaux, G., Blanc, G., 2003. The behaviour of arsenic in muddy
430 sediments of the Bay of Biscay (France). Geochim. Cosmochim. Ac. 67, 2993-3003.
431 Chen, C., Li, L., Huang, K., Zhang, J., Xie, W.Y., Lu, Y., Dong, X., Zhao, F.J., 2019. Sulfate-reducing
432 bacteria and methanogens are involved in arsenic methylation and demethylation in paddy soils. ISME
433 J. 13, 2523-2535.
434 Chen, Z., Kim, K.W., Zhu, Y.G., McLaren, R., Liu, F., He, J.Z., 2006. Adsorption (AsIII, V) and
435 oxidation (AsIII) of arsenic by pedogenic Fe–Mn nodules. Geoderma 136, 566-572.

436 Darland, J.E., Inskeep, W.P., 1997. Effects of pH and phosphate competition on the transport of
437 arsenate. J. Environ. Qual. 26, 1133-1139.
438 Das, S., Liu, C.C., Jean, J.S., Lee, C.C., Yang, H.J., 2016. Effects of microbially induced
439 transformations and shift in bacterial community on arsenic mobility in arsenic-rich deep aquifer
440 sediments. J. Hazard. Mater. 310, 11-19.
441 Di, X., Wei, W., Shiming, D., Qin, S., Chaosheng, Z., 2012. A high-resolution dialysis technique for
442 rapid determination of dissolved reactive phosphate and ferrous iron in pore water of sediments. Sci.
443 Total Environ. 421-422, 245-252.
444 Ding, S., Wang, Y., Wang, D., Li, Y.Y., Gong, M., Zhang, C., 2016. *In situ*, high-resolution evidence for
445 iron-coupled mobilization of phosphorus in sediments. Sci. Rep. 6, 24341.
446 Dočekalová, H., Clarisse, O., Salomon, S., Wartel, M., 2002. Use of constrained DET probe for a
447 high-resolution determination of metals and anions distribution in the sediment pore water. Talanta 57,
448 145-155.
449 Frenzel, P., Rothfuss, F., Conrad, R., 1992. Oxygen profiles and methane turnover in a flooded rice
450 microcosm. Biol. Fert. Soils 14, 84-89.
451 Gallagher, P.A., Schwegel, C.A., Wei, X., Creed, J.T., 2001. Speciation and preservation of inorganic
452 arsenic in drinking water sources using EDTA with IC separation and ICP-MS detection. J. Environ.
453 Monitor. 3, 371-376.
454 Gao, Y., Leermakers, M., Gabelle, C., Divis, P., Billon, G., Ouddane, B., Fischer, J.C., Wartel, M.,
455 Baeyens, W., 2006. High-resolution profiles of trace metals in the pore waters of riverine sediment
456 assessed by DET and DGT. Sci. Total Environ. 362, 266-277.

457 Gorny, J., Billon, G., Lesven, L., Dumoulin, D., Madé, B., Noiriel, C., 2015. Arsenic behavior in river
458 sediments under redox gradient: a review. Sci. Total Environ. 505, 423-434.
459 Grafe, M., Eick, M., Grossl, P., 2001. Adsorption of arsenate (V) and arsenite (III) on goethite in the
460 presence and absence of dissolved organic carbon. Soil Sci. Soc. Am. J. 65, 1680-1687.
461 Gustave, W., Yuan, Z.F., Ren, Y.X., Sekar, R., Chen, Z., 2019a. Arsenic alleviation in rice by using
462 paddy soil microbial fuel cells. Plant Soil 441, 111-127.
463 Gustave, W., Yuan, Z.F., Sekar, R., Ren, Y.X., Chang, H.C., Liu, J.Y., Chen, Z., 2018. The change in
464 biotic and abiotic soil components influenced by paddy soil microbial fuel cells loaded with various
465 resistances. J. Soil. Sediment. 19, 106-115.
466 Gustave, W., Yuan, Z.F., Sekar, R., Ren, Y.X., Liu, J.Y., Zhang, J., Chen, Z., 2019b. Soil organic matter
467 amount determines the behavior of iron and arsenic in paddy soil with microbial fuel cells.
468 Chemosphere 237, 124459.
469 Honma, T., Ohba, H., Kaneko-Kadokura, A., Makino, T., Nakamura, K., Katou, H., 2016. Optimal soil
470 Eh, pH, and water management for simultaneously minimizing arsenic and cadmium concentrations in
471 rice grains. Environ. Sci. Technol. 50, 4178-4185.
472 Hu, P., Ouyang, Y., Wu, L., Shen, L., Luo, Y., Christie, P., 2015. Effects of water management on
473 arsenic and cadmium speciation and accumulation in an upland rice cultivar. J. Environ. Sci. 27,
474 225-231.
475 Islam, F.S., Gault, A.G., Boothman, C., Polya, D.A., Charnock, J.M., Chatterjee, D., Lloyd, J.R., 2004.
476 Role of metal-reducing bacteria in arsenic release from Bengal delta sediments. Nature 430, 68-71.
477 Kazi, T.G., Brahman, K.D., Baig, J.A., Afridi, H.I., 2018. A new efficient indigenous material for

simultaneous removal of fluoride and inorganic arsenic species from groundwater. J. Hazard. Mater. 357, 159-167.

Khan, M.A., Stroud, J.L., Zhu, Y.G., McGrath, S.P., Zhao, F.J., 2010. Arsenic bioavailability to rice is elevated in Bangladeshi paddy soils. Environ. Sci. Technol. 44, 8515-8521.

Kumar, M., Ramanathan, A., Rahman, M.M., Naidu, R., 2016. Concentrations of inorganic arsenic in groundwater, agricultural soils and subsurface sediments from the middle Gangetic plain of Bihar, India. Sci. Total Environ. 573, 1103-1114.

Liu, F., 2006. Arsenite oxidation by three types of manganese oxides. J. Environ. Sci. 18, 292-298.

Lock, A., Wallschläger, D., Belzile, N., Spiers, G., Gueguen, C., 2018. Rates and processes affecting As speciation and mobility in lake sediments during aging. J. Environ. Sci. 66, 338-347.

Ma, W.W., Zhu, M.X., Yang, G.P., Li, T., 2017. In situ, high-resolution DGT measurements of dissolved sulfide, iron and phosphorus in sediments of the East China Sea: Insights into phosphorus mobilization and microbial iron reduction. Mar. Pollut. Bull. 124, 400-410.

Masscheleyn, P.H., Delaune, R.D., Patrick Jr, W.H., 1991. Effect of redox potential and pH on arsenic speciation and solubility in a contaminated soil. Environ. Sci. Technol. 25, 1414-1419.

Meharg, A.A., 2004. Arsenic in rice–understanding a new disaster for South-East Asia. Trends Plant Sci. 9, 415-417.

Mitsunobu, S., Toda, M., Hamamura, N., Shiraishi, F., Tominaga, Y., Sakata, M., 2020. Millimeter-scale topsoil layer blocks arsenic migration in flooded paddy soil. Geochim. Cosmochim. Ac. 274, 211-227.

Mucci, A., Richard, L.F., Lucotte, M., Guignard, C., 2000. The differential geochemical behavior of

499 arsenic and phosphorus in the water column and sediments of the Saguenay Fjord estuary, Canada.
500 Aquat. Geochem. 6, 293-324.
501 Myers, C.R., Nealson, K.H., 1988. Microbial reduction of manganese oxides: Interactions with iron
502 and sulfur. Geochim. Cosmochim. Ac. 52, 2727-2732.
503 Pester, M., Knorr, K.H., Friedrich, M.W., Wagner, M., Loy, A., 2012. Sulfate-reducing microorganisms
504 in wetlands–fameless actors in carbon cycling and climate change. Front. Microbiol. 3, 72.
505 Polizzotto, M.L., Kocar, B.D., Benner, S.G., Sampson, M., Fendorf, S., 2008. Near-surface wetland
506 sediments as a source of arsenic release to ground water in Asia. Nature 454, 505-508.
507 Roberts, L.C., Hug, S.J., Voegelin, A., Dittmar, J., Kretzschmar, R., Wehrli, B., Saha, G.C.,
508 Badruzzaman, A.B.M., Ali, M.A., 2010. Arsenic dynamics in porewater of an intermittently irrigated
509 paddy field in Bangladesh. Environ. Sci. Technol. 45, 971-976.
510 Shakoor, M., Niazi, N., Bibi, I., Rahman, M., Naidu, R., Dong, Z., Shahid, M., Arshad, M., 2015.
511 Unraveling health risk and speciation of arsenic from groundwater in rural areas of Punjab, Pakistan.
512 Int. J. Environ. Res. Pub. He. 12, 12371-12390.
513 Somenahally, A.C., Hollister, E.B., Yan, W., Gentry, T.J., Loeppert, R.H., 2011. Water management
514 impacts on arsenic speciation and iron-reducing bacteria in contrasting rice-rhizosphere compartments.
515 Environ. Sci. Technol. 45, 8328-8335.
516 Suda, A., Makino, T., 2016. Functional effects of manganese and iron oxides on the dynamics of trace
517 elements in soils with a special focus on arsenic and cadmium: a review. Geoderma 270, 68-75.
518 Suzuki, Y., Shimoda, Y., Endo, Y., Hata, A., Yamanaka, K., Endo, G., 2009. Rapid and effective
519 speciation analysis of arsenic compounds in human urine using anion-exchange columns in

520 HPLC-ICP-MS. J. Occup. Health 51, 380-385.
521 Takahashi, Y., Minamikawa, R., Hattori, K.H., Kurishima, K., Kihou, N., Yuita, K., 2004. Arsenic
522 behavior in paddy fields during the cycle of flooded and non-flooded periods. Environ. Sci. Technol. 38,
523 1038-1044.
524 Tong, H., Liu, C., Hao, L., Swanner, E.D., Chen, M., Li, F., Xia, Y., Liu, Y., Liu, Y., 2019. Biological
525 Fe(II) and As(III) oxidation immobilizes arsenic in micro-oxic environments. Geochim. Cosmochim.
526 Ac. 265, 96-108.
527 Tufano, K.J., Reyes, C., Saltikov, C.W., Fendorf, S., 2008. Reductive processes controlling arsenic
528 retention: revealing the relative importance of iron and arsenic reduction. Environ. Sci. Technol. 42,
529 8283-8289.
530 Tufano, K.J., Scott, F., 2008. Confounding impacts of iron reduction on arsenic retention. Environ. Sci.
531 Technol. 42, 4777-4783.
532 Violante, A., Pigna, M., 2002. Competitive sorption of arsenate and phosphate on different clay
533 minerals and soils. Soil Sci. Soc. Am. J. 66, 1788-1796.
534 Wang, H.Y., Byrne, J.M., Perez, J.P.H., Thomas, A.N., Göttlicher, J., Höfer, H.E., Mayanna, S., Kontny,
535 A., Kappler, A., Guo, H.M., Benning, L.G., Norra, S., 2020a. Arsenic sequestration in pyrite and
536 greigite in the buried peat of As-contaminated aquifers. Geochim. Cosmochim. Ac. 284, 107-119.
537 Wang, J., Kerl, C.F., Hu, P., Martin, M., Mu, T., Brüggenwirth, L., Wu, G., Said-Pullicino, D., Romani,
538 M., Wu, L., 2020b. Thiolated arsenic species observed in rice paddy pore waters. Nature Geosci. 13,
539 282-287.
540 Wang, M., Tang, Z., Chen, X.P., Wang, X., Zhou, W.X., Tang, Z., Zhang, J., Zhao, F.J., 2019. Water

management impacts the soil microbial communities and total arsenic and methylated arsenicals in rice grains. Environ. Pollut. 247, 736-744.

Weber, F.A., Hofacker, A.F., Voegelin, A., Kretzschmar, R., 2010. Temperature dependence and coupling of iron and arsenic reduction and release during flooding of a contaminated soil. Environ. Sci. Technol. 44, 116-122.

White, B.P., Mulligan, S., Merrill, K., Wright, J., 2007. An examination of the relationships between motor and process skills and scores on thes sensory profile. Appl. Environ. Microb. 61, 154-160.

Widerlund, A., Davison, W., 2007. Size and density distribution of sulfide-producing microniches in lake sediments. Environ. Sci. Technol. 41, 8044-8049.

Williams, P.N., Zhang, H., Davison, W., Meharg, A.A., Hossain, M., Norton, G.J., Brammer, H., Islam, M.R., 2011. Organic matter-solid phase interactions are critical for predicting arsenic release and plant uptake in Bangladesh paddy soils. Environ. Sci. Technol. 45, 6080-6087.

Wu, Z., Jiao, L., Wang, S., Xu, Y., 2016a. Multi-metals measured at sediment–water interface (SWI) by diffusive gradients in thin films (DGT) technique for geochemical research. Arch. Environ. Con. Tox. 70, 429-437.

Wu, Z., Ren, D., Zhou, H., Hang, G., Li, J., 2016b. Sulfate reduction and formation of iron sulfide minerals in nearshore sediments from Qi'ao Island, Pearl River Estuary, Southern China. Quatern. Int. 452, 137-147.

Xiu, W., Guo, H., Shen, J., Liu, S., Ding, S., Hou, W., Ma, J., Dong, H., 2016. Stimulation of Fe (II) oxidation, biogenic lepidocrocite formation, and arsenic immobilization by Pseudogulbenkiania sp. strain 2002. Environ. Sci. Technol. 50, 6449-6458.

562 Xu, W., Wang, H., Liu, R., Zhao, X., Qu, J., 2011. Arsenic release from arsenic-bearing Fe–Mn binary
563 oxide: Effects of Eh condition. Chemosphere 83, 1020-1027.
564 Xu, X., Chen, C., Wang, P., Kretzschmar, R., Zhao, F.J., 2017. Control of arsenic mobilization in paddy
565 soils by manganese and iron oxides. Environ. Pollut. 231, 37-47.
566 Yuan, Z.-F., Gustave, W., Sekar, R., Bridge, J., Wang, J.-Y., Feng, W.-J., Guo, B., Chen, Z., 2021.
567 Simultaneous measurement of aqueous redox-sensitive elements and their species across the soil-water
568 interface. J. Environ. Sci. 102, 1-10.
569 Yuan, Z.F., Ata-Ul-Karim, S.T., Cao, Q., Lu, Z., Cao, W., Zhu, Y., Liu, X., 2016. Indicators for
570 diagnosing nitrogen status of rice based on chlorophyll meter readings. Field Crops Res. 185, 12-20.
571 Yuan, Z.F., Gustave, W., Bridge, J., Liang, Y., Sekar, R., Boyle, J., Jin, C.Y., Pu, T.Y., Ren, Y.X., Chen,
572 Z., 2019. Tracing the dynamic changes of element profiles by novel soil porewater samplers with
573 ultralow disturbance to soil–water interface. Environ. Sci. Technol. 53, 5124-5132.
574 Zachara, J.M., Kukkadapu, R.K., Fredrickson, J.K., Gorby, Y.A., Smith, S.C., 2002. Biomineralization
575 of poorly crystalline Fe(III) oxides by dissimilatory metal reducing bacteria (DMRB). Geomicrobiol. J.
576 19, 179-207.
577 Zhang, H., Selim, H.M., 2008. Competitive sorption-desorption kinetics of arsenate and phosphate in
578 soils. Soil Sci. 173, 3-12.
579 Zhang, J., Ma, T., Yan, Y., Xie, X., Abass, O.K., Liu, C., Zhao, Z., Wang, Z., 2018. Effects of Fe-S-As
580 coupled redox processes on arsenic mobilization in shallow aquifers of Datong Basin, northern China.
581 Environ. Pollut. 237, 28-38.
582 Zhao, Y., Su, J., Ye, J., Rensing, C., Tardif, S., Zhu, Y., Brandt, K.K., 2019. AsChip: a high-throughput

583 qPCR chip for comprehensive profiling of genes linked to microbial cycling of arsenic. Environ. Sci.
584 Technol. 53, 798-807.
585 Zheng, J., Hintelmann, H., Dimock, B., Dzurko, M.S., 2003. Speciation of arsenic in water, sediment,
586 and plants of the Moira watershed, Canada, using HPLC coupled to high resolution ICP–MS. Anal.
587 Bioanal. Chem. 377, 14-24.
588 Zobrist, J., Dowdle, P.R., Davis, J.A., Oremland, R.S., 2000. Mobilization of arsenite by dissimilatory
589 reduction of adsorbed arsenate. Environ. Sci. Technol. 34, 4747-4753.